Structural deformation, strength, and instability of cubic BN compared to diamond: A first-principles study

Yi Zhang,[1] Hong Sun,[1,2,*] and Changfeng Chen[2,*]
[1]*Department of Physics, Shanghai Jiao Tong University, Shanghai 200030, China*
[2]*Department of Physics and High Pressure Science and Engineering Center, University of Nevada, Las Vegas, Nevada 89154, USA*
(Received 4 January 2006; revised manuscript received 24 February 2006; published 28 April 2006)

Cubic boron nitride (*c*-BN) is the second (only to diamond) hardest material with superior thermal stability. Despite its wide range of applications as a superhard material, the structural deformation modes of *c*-BN at the atomistic level are still not well understood. In this paper, we report first-principles calculations on its structural deformation, strength, and lattice instabilities under large tensile and shear strains. Calculations are also performed for diamond to extend previous results for a systematic comparison with *c*-BN. We examine the atomistic bonding structural change and analyze the calculated stress-strain relations for a microscopic understanding of the deformation modes. Both *c*-BN and diamond show essentially isotropic elastic response at small strains under tensile and shear deformation. At larger strains, anisotropies in the stress response develop, yielding significantly different peak stresses along different tensile and shear directions. It results in a strong tendency for tensile fractures in the (111) planes in both materials. The local bonding structural relaxation modes are analyzed to understand the large anisotropies in the tensile peak stresses in different crystallographic directions and to explain the quantitative differences between *c*-BN and diamond in their stress-strain relations. A simple rule is suggested for determining the direction of the weakest tensile strength for similar covalent solids. Under large shear deformation, the bond breaking in *c*-BN leads to a graphitic phase with an orientation different from that in diamond. Its atomistic origin and possible consequences on the mechanical property are discussed.

DOI: 10.1103/PhysRevB.73.144115 PACS number(s): 62.20.−x, 63.20.Dj, 71.15.Mb

I. INTRODUCTION

Crystalline boron nitrides (BN) have attracted considerable interest over the years. Many experimental investigations have reported their synthesis and characterization.[1–9] Theoretical studies with increasing accuracies have been performed to examine the properties of the equilibrium structures of various crystalline forms of BN.[10–15] Among them the cubic BN (*c*-BN) has received the most attention since it is second only to diamond in hardness and exceeds diamond in thermal stability. These properties make it highly desirable in many microelectronic and tooling applications. One of the most important aspects in these applications is its structural response to external loading conditions, including compressive, tensile, shear, as well as more complicated stress fields such as the triaxial stress field in nanoindentation. An earlier work established the volume compression equation of state for cubic boron nitride under hydrostatic pressure.[16] However, despite its wide range of applications as a superhard material, there is still a lack of a full understanding for its stress-strain relation and the deformation process associated with the mechanical failure modes under large tensile and shear strains. A microscopic understanding of these important structural behavior became available recently for diamond.[17,18] The close similarities in the structural and bonding characters between diamond and cubic BN may lead to the expectation that the deformation processes and failure modes in these two materials should also be similar. However, it was shown[19] that the bond softening behavior in *c*-BN can be different from that in diamond. It calls for a more systematic quantitative examination of the structural deformation in *c*-BN. Additional calculations for diamond are also needed for a more detailed understanding of its structural properties.

In this paper, we report on a first-principles study on the stress-strain relation of *c*-BN under large tensile and shear strains that extends the results we recently reported.[19] We carried out calculations to establish the detailed atomistic bond softening and breaking modes in *c*-BN and further examine the corresponding behavior in diamond for a close comparison. The calculated results show that *c*-BN indeed shares with diamond some similarities in its structural deformation behavior; but the calculations also reveal interesting differences in their bond softening and breaking modes. We systematically examined the stress response to tensile strains in the principal symmetry directions and the associated variations of the bond length and bond angle for a microscopic understanding of the underlying mechanism. We also obtained in *c*-BN a shear deformation mode that is distinctive from that in diamond. It leads to a different bond breaking pattern in the transition from the cubic structure to a graphitelike layered structure under large shear stresses. Such a shear driven cubic-to-layered structural transition was recently observed in diamond during an nanoindentation measurement.[20] It is expected that the shear deformation mode in *c*-BN should manifest itself in a similar setting and that its different bond breaking mode may lead to different mechanical responses in applications where the deformation is predominantly shear in nature. The results of the present work offer insights into the atomistic origin of the structural response to large tensile and shear strains in *c*-BN and diamond.

II. METHOD OF CALCULATION

The total-energy calculations were carried out using the local-density-approximation (LDA) pseudopotential scheme with a plane-wave basis set.[21–23] The norm-conserving Troullier-Martins pseudopotentials[24] were used with cutoff radii of 1.3, 1.3, and 1.5 a.u. for C, N, and B, respectively. The exchange-correlation functional of Ceperley and Alder[22] as parametrized by Perdew and Zunger[25] was used. The total energy of the structures was minimized by relaxing the structural parameters using a quasi-Newton method.[26] An $8\times8\times8$ Monkhorst-Pack[27] k-point grid and an 80 Ry energy cutoff were used in the calculations. This approach has been widely used to calculate the properties of crystalline solids with good accuracy. It was employed to calculate the equilibrium structural properties of diamond and cubic BN and produced the lattice constant and elastic muduli within 1% and a few percent, respectively, compared to experiments.[28] The error in the calculated stresses due to the energy cutoff and k-point grid was less than 0.1 GPa based on convergence tests. The quasistatic ideal strength and relaxed loading path in the various directions was determined using a method described previously.[29,30] The lattice vectors were incrementally deformed in the direction of the applied stress. At each step the atomic basis vectors and all the strain components orthogonal to the applied stress were simultaneously relaxed. The residual orthogonal components of the Hellmann-Feynman stress tensor are less than 0.1 GPa. The shape of the unit cell is determined by this process without any externally imposed boundary conditions. The tensile stresses along three principal symmetry crystallographic directions and the shear stresses in the easy slip planes were calculated. This approach with a relaxed loading path has been successfully applied to the calculation of the strength of several strong solids.[29–31] In the present work, we employ this approach to carry out a detailed study of the structural response to large tensile and shear strains in c-BN in close comparison to diamond. We also carried out dynamic phonon calculations using the ABINIT code[32] to test the stability of the strained structures up to the peak stress where the elastic instability occurs. The results confirm that, in all the cases studied in the present work, there are no inhomogeneous structural instability due to dynamic phonon softening that could intrude before the materials become unstable according to the elastic stability criteria,[33–35] and the calculated peak strain marks the onset of the elastic instability in each case under the specified deformation mode.

III. RESULTS AND DISCUSSION

Figure 1 shows the calculated stress-strain relation for c-BN under tensile strains in three principal symmetry crystallographic directions. We also performed calculations for diamond; the data, which are in excellent agreement with the results of the previous calculation,[17] are included in Fig. 1 for comparison. The calculated results clearly show that c-BN shares with diamond some important features in their response to uniaxial tensile deformations. They both exhibit strong anisotropies in their peak tensile stresses, with descending magnitudes for ⟨100⟩, ⟨110⟩, and ⟨111⟩ directions at

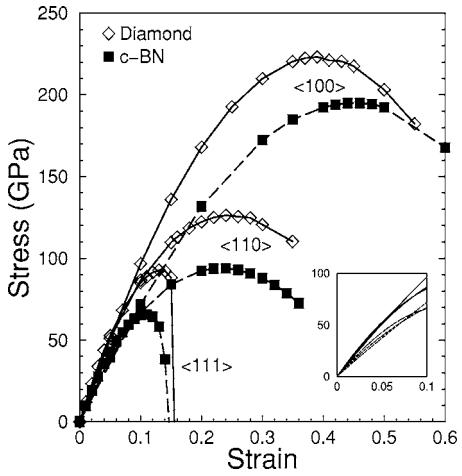

FIG. 1. The calculated tensile stress-strain relation for diamond and c-BN in the three principal symmetry crystallographic directions. The peak stresses are 223 GPa, 126 GPa, and 93 GPa in ⟨100⟩, ⟨110⟩, and ⟨111⟩ directions, respectively, for diamond, which are in excellent agreement with the previously reported data of 225 GPa, 130 GPa, and 90 GPa (Ref. 17). The corresponding peak stresses for c-BN are 195 GPa, 94 GPa, and 66 GPa. The strains corresponding to these peak stresses are 0.39, 0.24, and 0.13 for diamond and 0.45, 0.23, and 0.11 for c-BN. The inset shows the tensile stress-strain relation for diamond (solid lines) and c-BN (dashed lines) at small strains to illustrate the nearly isotropic stress response to tensile strains.

the ratios of 2.40:1.35:1.00 for diamond and 3.00:1.45:1.00 for cubic BN. This large orientational anisotropy in peak tensile stress was cited to explain the strong tendency for diamond crystals to cleave in the ⟨111⟩ planes.[17] The present results indicate that the tendency for the ⟨111⟩ cleavage in cubic BN is even stronger. Similar to the situation in diamond, tensile fracture in c-BN should occur along the {111} planes even when the stress is applied uniaxially at a large angle to the {111} since the resolved stress on {111} still will cause fracture in these easy cleavage planes before bond breaking would occur in other planes given the large ratios of the peak stresses. Another interesting observation is that both materials show nearly *isotropic* stress response under small tensile strains (see the inset in Fig. 1), despite the large anisotropies in their peak stresses along the different crystallographic directions. It indicates that an isotropic elastic model, like those used in the engineering modeling,[36] can provide a reasonably good description for the structural response in diamond and c-BN under tensile deformations as long as its application is restricted to processes involving strains that are not too large. Meanwhile, it is noticed that at small strains the slopes of the stress-strain curves for cubic BN show larger variations compared to diamond, with its ⟨111⟩ stress response initially stronger than those in the ⟨110⟩ and ⟨100⟩ directions.

The results in Fig. 1 also reveal interesting differences between diamond and cubic BN in their response to tensile strains. It is noted that the initially strong stress response of c-BN in the ⟨111⟩ direction quickly deteriorates, leading to an early bond softening with a significant reduction in the ideal tensile strength, defined as the minimum critical stress

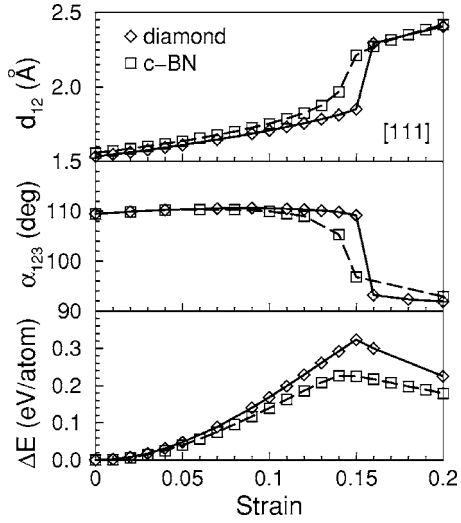

FIG. 2. The calculated [111] bond length d_{12}, the bond angle α_{123} between the [111] and $11\bar{1}$ bonds, and the corresponding strain energy of diamond and *c*-BN under the uniaxial [111] tensile strain. The index numbers in the subscripts of the bond length and angle above refer to the position of atoms indicated in Fig. 3

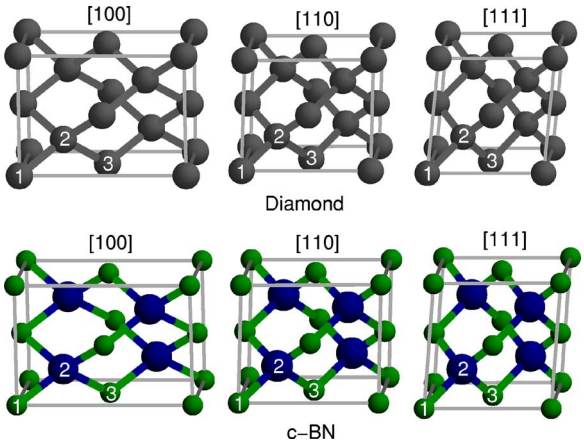

FIG. 3. (Color online) The snapshots of the calculated diamond (top row) and *c*-BN (bottom row) structures at the elastic limit under the tensile stresses along the three principal symmetry directions. The corresponding strains in the [100], [110], and [111] directions are 0.39, 0.24, and 0.13 for diamond and 0.45, 0.23, and 0.11 for *c*-BN. The [100] and [001] directions point to the right and up, respectively, in the figure.

(in the ⟨111⟩ direction in the present case) at which a perfect crystal becomes mechanically unstable.[37,38] In contrast, the C–C bonds in diamond remain strong up to the cubic-to-graphitic transition point with much less preceding bond softening. For an understanding of the structural response at the atomistic level, it is instructive to examine the bond length as a function of the ⟨111⟩ tensile strain as shown in Fig. 2. It is clearly seen that the length of the ⟨111⟩ C–C bonds increases with the strain at a lower rate with a big jump at the cubic-to-graphitic transformation point (at about 15% strain), whereas the length of the ⟨111⟩ B-N bonds increases at a higher rate with a much more gradual change during its cubic-to-graphitic transformation. Here the dominant structural deformation mode is direct elongation of the ⟨111⟩ bonds aligned in the direction of the applied stress. The length variation of the bonds in the {111} planes (not shown) is minimal. Figure 2 also shows the angle between the [111] bond and the $[11\bar{1}]$ bond; the angle variation is small under the strain until near the bond breaking point corresponding to the cubic-to-graphitic transformation. Therefore, under the ⟨111⟩ tensile deformation, the stress response in *c*-BN and diamond is almost entirely attributed to the direct uniaxial bond stretch. We also calculated the strain energy associated with the ⟨111⟩ tensile deformation. The results presented in Fig. 2 show that diamond has a higher energy barrier of 0.32 eV/atom for the cubic-to-graphitic transformation, reflecting its strong covalent C–C bonds that are hard to break; meanwhile, *c*-BN with a partial ionic bonding has a lower energy barrier of 0.22 eV/atom, indicating that it is more susceptible to the structural change.

Under the ⟨110⟩ and ⟨100⟩ strains, *c*-BN is structurally much more durable not only in comparison to its own ⟨111⟩ data but also relative to the diamond data under the same strains. As shown in Fig. 1, the peak stress for *c*-BN occurs at about the same strain as that for diamond under the ⟨110⟩ tensile strain and at a much larger strain compared to diamond under the ⟨100⟩ tensile strain. To understand this increase in the range of elasticity in *c*-BN, especially relative to that of diamond under the same strain, we examine the atomistic bonding structural relaxation modes. Unlike the ⟨111⟩ tensile case where direct bond stretch is practically the only relaxation mode, under the ⟨110⟩ and ⟨100⟩ tensile stresses, another structural relaxation mode becomes available, namely the relaxation of the bond angle. Since there are no bonds aligned in the direction of the applied stress here (see Fig. 3), the bond angle relaxation plays an effective and important role in the overall structural response. Here the [111] bond is the long bond that stretches the most (in the [100] case, all bonds stretch equally). The calculated [111] bond length, d_{12}, and the bond angle between the [111] and the $[11\bar{1}]$ bond, α_{123}, are plotted in Fig. 4 (for [110] strain) and Fig. 5 (for [100] strain). It is obvious that both the bond length and the bond angle respond to the applied stress with smooth and continuous changes in the entire range of strain. A close examination reveals the role of the two relaxation modes at different stages of the deformation. The rate of increase of the bond angle is at a higher rate initially at small strains and then at decreasing rates as the strain increases; meanwhile the opposite occurs for the bond elongation. Under the [110] strain, the bond length variation of both *c*-BN and diamond has nearly identical rate of increase, but *c*-BN has a larger amount of bond angle relaxation. Under the [100] strain, the increase of the [111] B–N bond is slower than the [111] C–C bond, accompanied by an larger increase in the bond angle in *c*-BN. In both cases, the strain energy rises smoothly, with the value for diamond increasing at a higher rate. Due to its significantly increased structural durability aided by the greater bond angle relaxation, the peak stresses of *c*-BN along these directions not only reach higher values, as do the corresponding data for diamond, but they also come closer to the values of diamond. The peak tensile stress of *c*-BN along the [100] is 87% of the value for dia-

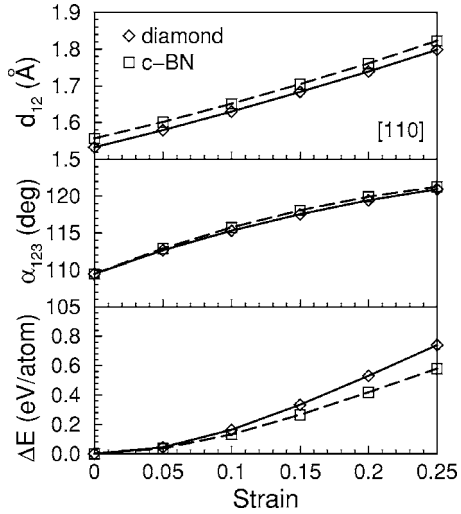

FIG. 4. The calculated [111] bond length d_{12}, the bond angle α_{123} between the [111] and [11$\bar{1}$] bonds, and the corresponding strain energy of diamond and *c*-BN under the uniaxial [110] tensile strain.

mond, while the ratios are 75% and 70% for the [110] and [111] directions, respectively. These results show that the tensile strength of *c*-BN relative to that of diamond has a fairly large range of variation, depending sensitively on the orientation of the uniaxial tensile deformation mode. This result also suggests a simple rule for determining the direction along which the ideal tensile strength is obtained in similar covalent solids. The ideal tensile strength, which is the minimum peak stress under tensile deformation, occurs in the direction where the applied stress would initially cause direct bond stretch with little other (e.g., angular) relaxation. This is consistent with the recent results on the ideal tensile strength of strong covalent solids cubic BC_2N (Ref. 31) and C_3N_4 (Ref. 39). This rule should be useful in the study of

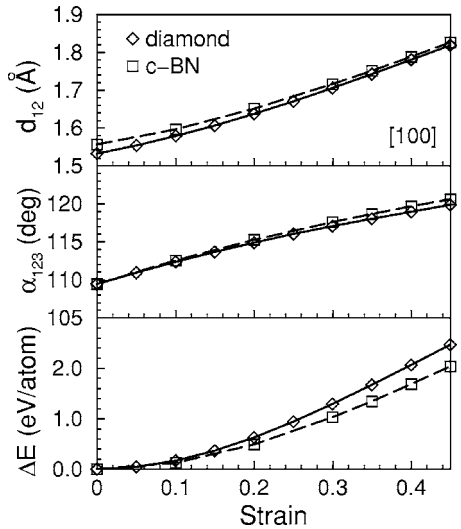

FIG. 5. The calculated [111] bond length d_{12}, the bond angle α_{123} between the [111] and [11$\bar{1}$] bonds, and the corresponding strain energy of diamond and *c*-BN under the uniaxial [100] tensile strain.

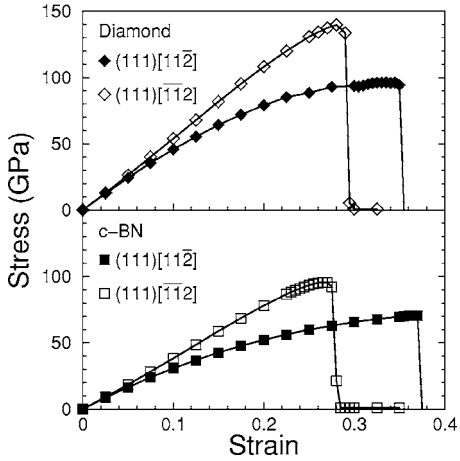

FIG. 6. The calculated shear stress-strain relation for diamond and *c*-BN in the ⟨111⟩ easy slip plane along the two inequivalent shear directions. The peak stresses are 96.3 GPa and 140 GPa under the (111)[11$\bar{2}$] and (111)[$\bar{1}$12] shear, respectively, for diamond, and 70.5 GPa and 95.5 GPa for *c*-BN. The strains corresponding to these peak stresses are 0.345 and 0.280 for diamond and 0.365 and 0.265 for *c*-BN.

materials with complex structures where the weakest direction under the tensile stress may not be obvious.

We now turn to the shear deformation in diamond and cubic BN. Figure 6 shows the calculated shear stress-strain relation. Both materials have the (111) easy slip plane for shear deformation. In the (111) planes, there are two inequivalent shear directions, (111)[11$\bar{2}$] and (111)[$\bar{1}$12]. They correspond to two sets of exactly opposite shear stresses in the (111) plane, but there is no reversal symmetry in this problem due to the anisotropic relative bonding orientation in the crystal structure. The results in Fig. 6 show that both *c*-BN and diamond exhibit large anisotropies in their peak shear stress under the two shear modes. The ratio of the peak stresses for *c*-BN is 95.5 GPa/70.5 GPa=1.35, which is slightly lower than the corresponding value of 140 GPa/96.3 GPa=1.45 for diamond. Despite these large anisotropies in the peak stresses, the stress-strain relations for both materials show an isotropic behavior at small strains with visible deviations start to occur at about 5% shear strain. Combined with the results of the tensile stress-strain relation discussed above, it is clear that an isotropic elastic model would provide a good description for both the tensile and shear deformation at small strains in diamond and *c*-BN. This provides an atomistic-level justification for the isotropic elastic description[36] of the diamond indenter used in nanoindentation measurements. This is applicable to situations where the deformation of the indenter is small either because the test surface is much softer than diamond or because the loading force is not too large. The present results on *c*-BN show that it can also be described by an isotropic elastic model at small tensile and shear strains may be useful in its structural modeling for certain engineering applications.

We next examine the bond length and the strain energy variation of *c*-BN and diamond under the two inequivalent shear deformation modes in the easy slip (111) plane. The results are presented in Figs. 7 and 8. Under the (111)[11$\bar{2}$]

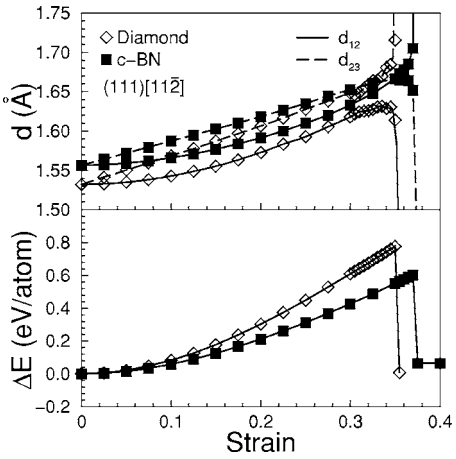

FIG. 7. The calculated length of the [111] (d_{12}) and [11$\bar{1}$] (d_{23}) bonds in c-BN and diamond under the (111)[11$\bar{2}$] shear. Also shown are the corresponding strain energies. See Fig. 9 for the snapshots of the shear strained structures and the atomic positions.

shear, both the [111] and [11$\bar{1}$] bonds increase until the cubic-to-graphitic transformation where the diamond [11$\bar{1}$] and the c-BN [111] bonds break and the diamond [111] bonds and the c-BN [11$\bar{1}$] bonds retract to the much shorter length in the graphitic sheets. It is noticed that the c-BN [11$\bar{1}$] bonds are actually the long bonds until very close to the transformation point where the c-BN [111] bonds quickly expand and break under the shear strain. This phenomenon of the switch of the long bonds under shear deformation has been observed before in diamond;[18] but it involves only different bonds in the (111) plane. Here in c-BN it involves the out-of-the-plane [111] bonds. The result is a qualitatively different shear breaking pattern with the graphitic sheets parallel to the (111) plane, whereas in the diamond case, the graphitic sheets are running perpendicular to the (111) plane (see Fig. 9). The origin of this phenomenon may lie in the strain induced charge redistribution that can be best investi-

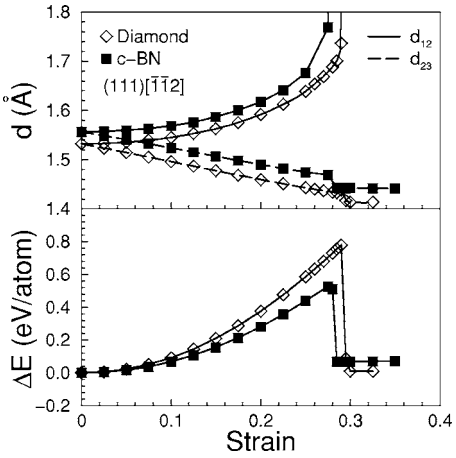

FIG. 8. The calculated length of the [111] (d_{12}) and [$\bar{1}$11] (d_{23}) bonds in c-BN and diamond under the (111)[$\bar{1}$12] shear. Also shown are the corresponding strain energies. See Fig. 9 for the snapshots of the shear strained structures and the atomic positions.

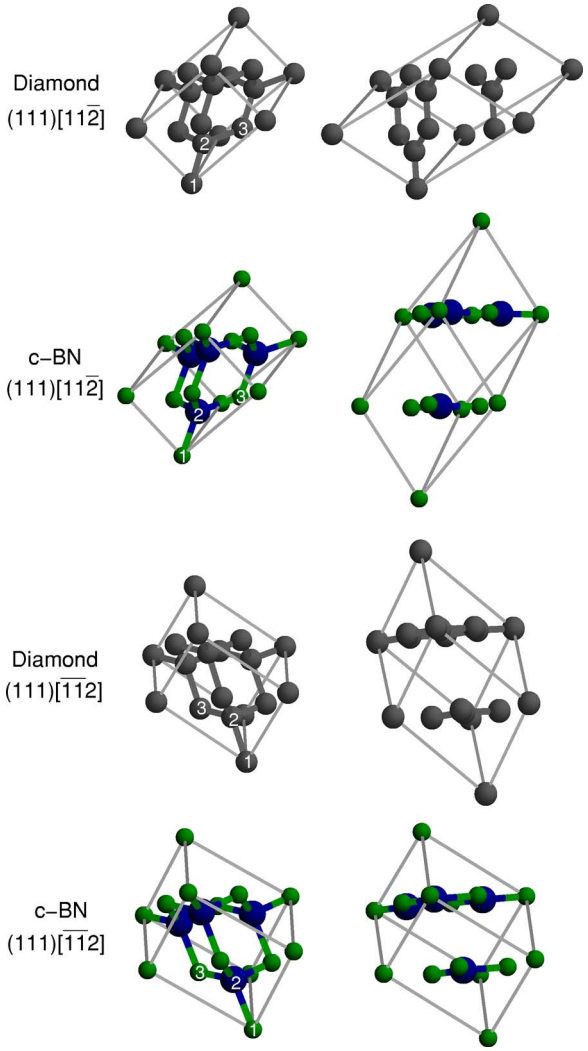

FIG. 9. (Color online) The snapshots of the calculated diamond and c-BN structures right before and after the cubic-to-graphitic transformation under the shear indicated to the left of the structures. The corresponding shear strains are 0.350 and 0.355 for diamond (111)[11$\bar{2}$], 0.370 and 0.375 for c-BN (111)[11$\bar{2}$], 0.290 and 0.295 for diamond (111)[$\bar{1}$12], and 0.275 and 0.280 for c-BN (111) ×[$\bar{1}$12]. Under the (111)[11$\bar{2}$] shear, both c-BN and diamond undergo an approximately 50% volume expansion right after the cubic-to-graphitic transformation; while under the (111)[$\bar{1}$12] shear, the initial volume of the graphitic phases are only 24% and 9%, respectively, larger than the critically strained diamond and c-BN structures, as shown in the figure, although they also reach close to 50% at slightly larger strains. The [111] and [11$\bar{2}$] directions point up and to the right, respectively, in the figure.

gated by a molecular dynamics simulation. It is noted that the alternating bond elongation that results in the switch of the long bond in c-BN under the (111)[11$\bar{2}$] shear also extends its range of elasticity to the shear strain of 0.365. This is larger than the corresponding value of 0.345 for diamond. In contrast, under the (111)[$\bar{1}$12] shear, the [111] bonds are consistently the long bonds in both c-BN and diamond. Consequently, the resulted graphitic structures for both materials have the same orientation with the graphitic sheets parallel to

the (111) plane (see Fig. 9). The lack of the multiple large bond elongation modes under the $(111)[\bar{1}\bar{1}2]$ shear limits the range of elasticity in *c*-BN to the shear strain of 0.265, which is smaller than the corresponding value of 0.280 for diamond. Moreover, under the $(111)[\bar{1}\bar{1}2]$ shear, the $[\bar{1}11]$ bonds are compressed from the start. This bond is aligned in the direction of the shear, just like the $[11\bar{1}]$ bond under the $(111)[11\bar{2}]$ shear. The lack of a reversal symmetry in the structure results in a very different bond variation mode. It also leads to much higher rates of strain energy increase and shorter ranges of elasticity for both materials. For diamond, the energy barriers reach about the same height of 0.8 eV/atom under the two shear deformation modes. For *c*-BN, the energy barrier under the $(111)[11\bar{2}]$ shear is higher due to the extended elastic range. However, despite the higher energy barrier, the $(111)[11\bar{2}]$ shear is still the preferred deformation mode since it requires much smaller stress to proceed and is more effective in causing the bond elongation and breaking. The different orientations for diamond and *c*-BN under this preferred shear deformation mode may have important implications for certain mechanical processes where a resolved uniaxial stress along the [111] direction, which is present in, for example, nanoindentation measurements, could induce much larger structural variation in *c*-BN. It should be noted that the graphitic structures of diamond and *c*-BN with the graphitic layers parallel or perpendicular to (111) resulting from the $(111)[11\bar{2}]$ or $(111)\times[\bar{1}\bar{1}2]$ shear breaking processes are not only both local minima, but also the same structure (with different orientations) after the full structural relaxation. The issue of which potential energy surface valley is preferred is determined by which bonds (parallel to [111] or $[11\bar{1}]$) break first under the shear strain. The increase of the strain in each step of our calculation is very small (0.005), which we believe is accurate enough to predict which bonds break first.

IV. SUMMARY

In summary, we have carried out first principles calculations to establish a systematic quantitative description of the tensile and shear deformation, strength, and lattice instability in cubic boron nitride in close comparison to diamond. The calculated results show some similarities shared by these two top superhard materials. These include their nearly isotropic stress response to small tensile and shear strains and the strong anisotropy in their peak stresses along different crystallographic directions. The calculations also reveal interesting differences between the two materials, most notably the differences in the bond softening pattern and the range of the bond durability under the tensile strain and the bond breaking pattern under the shear strain. We examined the atomistic bonding structural variations and the associated energetics to elucidate the microscopic mechanism for the obtained stress-strain relation of cubic BN and diamond. These results offer a detailed description of their structural properties under the tensile and simple shear deformation, which may also provide valuable information for the simulation and analysis of their structural response under more complex loading conditions.

ACKNOWLEDGMENTS

This work was supported by the DOE under Cooperative Agreement No. DE-FC52-01NV14049. H. S. was also supported by the National Natural Science Foundation of China (Grant No. 10574089 and 50532020) and the High Performance Computing Center at Shanghai Jiao Tong University.

*To whom correspondence should be addressed. Electronic address: hsun@sjtu.edu.cn; chen@physics.unlv.edu

[1] F. R. Bundy and R. H. Wentorg, Jr., J. Chem. Phys. **38**, 1144 (1963).
[2] F. R. Bundy and J. S. Kasper, J. Chem. Phys. **46**, 3437 (1967).
[3] F. R. Corrigan and F. P. Bundy, J. Chem. Phys. **63**, 3812 (1975).
[4] V. L. Solozhenko, Diamond Relat. Mater. **4**, 1 (1994).
[5] V. L. Solozhenko, J. Hard Mater. **6**, 51 (1995).
[6] S. Bohr, R. Haubner, and B. Lux, Diamond Relat. Mater. **4**, 714 (1995).
[7] C. S. Yoo, J. Akella, H. Cynn, and M. Nicol, Phys. Rev. B **56**, 140 (1997).
[8] H. Sachdev, R. Haubner, H. Noth, and B. Lux, Diamond Relat. Mater. **6**, 286 (1997).
[9] V. L. Solozhenko, V. Z. Turkevich, and W. B. Holzapfel, J. Phys. Chem. B **103**, 2903 (1999).
[10] J. Furthmüller, J. Hafner, and G. Kresse, Phys. Rev. B **50**, 15606 (1994).
[11] K. Albe, Phys. Rev. B **55**, 6203 (1997).
[12] G. Kern, G. Kresse, and J. Hafner, Phys. Rev. B **59**, 8551 (1999).
[13] A. Janotti, S.-H. Wei, and D. J. Singh, Phys. Rev. B **64**, 174107 (2001).
[14] W. J. Yu, W. M. Lau, S. P. Chan, Z. F. Liu, and Q. Q. Zheng, Phys. Rev. B **67**, 014108 (2003).
[15] E. Kim and C. F. Chen, Phys. Lett. A **319**, 384 (2003).
[16] E. Knittle, R. M. Wentzcovitch, R. Jeanloz, and M. L. Cohen, Nature (London) **337**, 349 (1989).
[17] R. H. Telling, C. J. Pickard, M. C. Payne, and J. E. Field, Phys. Rev. Lett. **84**, 5160 (2000).
[18] H. Chacham and L. Kleinman, Phys. Rev. Lett. **85**, 4904 (2000).
[19] Y. Zhang, H. Sun, and C. F. Chen, Phys. Rev. Lett. **94**, 145505 (2005).
[20] Y. G. Gogotsi, A. Kaiter, and K. G. Nickel, Nature (London) **401**, 664 (1999).
[21] J. Ihm, A. Zunger, and M. L. Cohen, J. Phys. C **12**, 4409 (1979).
[22] D. M. Ceperley and B. J. Alder, Phys. Rev. Lett. **45**, 566 (1980).
[23] M. L. Cohen, Phys. Scr., T **1**, 5 (1982).
[24] N. Troullier and J. L. Martins, Phys. Rev. B **43**, 1993 (1991).
[25] J. P. Perdew and A. Zunger, Phys. Rev. B **23**, 5048 (1981).
[26] B. G. Pfrommer, M. Cote, S. G. Louie, and M. L. Cohen, J.

Comput. Phys. **131**, 233 (1997).
[27] H. J. Monkhorst and J. D. Pack, Phys. Rev. B **13**, 5188 (1976).
[28] H. Sun, S. H. Jhi, D. Roundy, M. L. Cohen, and S. G. Louie, Phys. Rev. B **64**, 094108 (2001).
[29] D. Roundy, C. R. Krenn, M. L. Cohen, and J. W. Morris, Jr., Philos. Mag. A **81**, 1725 (2001).
[30] D. Roundy, C. R. Krenn, M. L. Cohen, and J. W. Morris, Jr., Phys. Rev. Lett. **82**, 2713 (1999).
[31] Y. Zhang, H. Sun, and C. F. Chen, Phys. Rev. Lett. **93**, 195504 (2004).
[32] X. Gonze, Phys. Rev. B **55**, 10337 (1997); X. Gonze and C. Lee, *ibid.* **55**, 10355 (1997).
[33] S. H. Jhi, S. G. Louie, M. L. Cohen, and J. W. Morris, Jr., Phys. Rev. Lett. **87**, 075503 (2001).
[34] J. Li and S. Yip, Comput. Model. Eng. Sci. **3**, 219 (2002).
[35] D. M. Clatterbuck, C. R. Krenn, M. L. Cohen, and J. W. Morris, Jr., Phys. Rev. Lett. **91**, 135501 (2003).
[36] W. C. Oliver and G. M. Pharr, J. Mater. Res. **7**, 1564 (1992).
[37] A. Kelly and N. H. Macmillan, *Strong Solids*, 3rd ed. (Clarendon, Oxford, 1986), pp. 1–56.
[38] J. W. Morris, Jr., C. R. Krenn, D. Roundy, and M. L. Cohen, in *Phase Transformations and Evolution in Materials*, edited by P. E. Turchi and A. Gonis (TMS, Warrendale, PA, 2000), pp. 187–207.
[39] Y. Zhang, H. Sun, and C. F. Chen, Phys. Rev. B **73**, 064109 (2006).